NAVAL POSTGRADUATE SCHOOL

MONTEREY, CALIFORNIA

THESIS

SEA-SURFACE SIGNATURES OF PROPAGATING SUBMERGED OBJECTS

by

Yeonwon Kim

September 2022

Thesis Advisor: Timour Radko
Second Reader: Justin M. Brown

Approved for public release. Distribution is unlimited.

THIS PAGE INTENTIONALLY LEFT BLANK

REPORT DOCUMENTATION PAGE	*Form Approved OMB No. 0704-0188*

1. AGENCY USE ONLY *(Leave blank)*	**2. REPORT DATE** September 2022	**3. REPORT TYPE AND DATES COVERED** Master's thesis

4. TITLE AND SUBTITLE
SEA-SURFACE SIGNATURES OF PROPAGATING SUBMERGED OBJECTS

5. FUNDING NUMBERS

6. AUTHOR(S) Yeonwon Kim

7. PERFORMING ORGANIZATION NAME(S) AND ADDRESS(ES)
Naval Postgraduate School
Monterey, CA 93943-5000

8. PERFORMING ORGANIZATION REPORT NUMBER

9. SPONSORING / MONITORING AGENCY NAME(S) AND ADDRESS(ES)
N/A

10. SPONSORING / MONITORING AGENCY REPORT NUMBER

11. SUPPLEMENTARY NOTES The views expressed in this thesis are those of the author and do not reflect the official policy or position of the Department of Defense or the U.S. Government.

12a. DISTRIBUTION / AVAILABILITY STATEMENT
Approved for public release. Distribution is unlimited.

12b. DISTRIBUTION CODE
A

13. ABSTRACT (maximum 200 words)

The recent development of various masking and noise-reducing technologies for submarines, aimed at the reduction of their acoustic signatures, makes it critical to advance and implement alternative detection methods. To meet this objective, this study explores the prospects of identification of turbulent wakes that are necessarily generated by propagating objects in the ocean. This project is based on a series of high-resolution numerical simulations that were performed using the CFD (computational fluid dynamics) software OpenFOAM. In particular, the analysis is focused on the sea-surface signatures of submarine wakes and the role played by the sub-surface mixed layer in the vertical transmission of hydrodynamic wake signals. In the course of this investigation, we systematically explore the sensitivity of wake dynamics and its detection potential to the mixed layer depth, the location of the submersible, and its speed. Our findings are expected to ultimately offer valuable operational guidance for Undersea Warfare.

14. SUBJECT TERMS
sea-surface signatures, submarines, submersibles, submerged objects

15. NUMBER OF PAGES
51

16. PRICE CODE

17. SECURITY CLASSIFICATION OF REPORT	**18. SECURITY CLASSIFICATION OF THIS PAGE**	**19. SECURITY CLASSIFICATION OF ABSTRACT**	**20. LIMITATION OF ABSTRACT**
Unclassified	Unclassified	Unclassified	UU

NSN 7540-01-280-5500

Standard Form 298 (Rev. 2-89)
Prescribed by ANSI Std. 239-18

THIS PAGE INTENTIONALLY LEFT BLANK

Approved for public release. Distribution is unlimited.

SEA-SURFACE SIGNATURES OF PROPAGATING SUBMERGED OBJECTS

Yeonwon Kim
So-ryeong, Republic of Korea Navy
BS, Republic of Korea Naval Academy, 2011

Submitted in partial fulfillment of the
requirements for the degree of

MASTER OF SCIENCE IN PHYSICAL OCEANOGRAPHY

from the

NAVAL POSTGRADUATE SCHOOL
September 2022

Approved by: Timour Radko
Advisor

Justin M. Brown
Second Reader

Peter C. Chu
Chair, Department of Oceanography

THIS PAGE INTENTIONALLY LEFT BLANK

ABSTRACT

The recent development of various masking and noise-reducing technologies for submarines, aimed at the reduction of their acoustic signatures, makes it critical to advance and implement alternative detection methods. To meet this objective, this study explores the prospects of identification of turbulent wakes that are necessarily generated by propagating objects in the ocean. This project is based on a series of high-resolution numerical simulations that were performed using the CFD (computational fluid dynamics) software OpenFOAM. In particular, the analysis is focused on the sea-surface signatures of submarine wakes and the role played by the sub-surface mixed layer in the vertical transmission of hydrodynamic wake signals. In the course of this investigation, we systematically explore the sensitivity of wake dynamics and its detection potential to the mixed layer depth, the location of the submersible, and its speed. Our findings are expected to ultimately offer valuable operational guidance for Undersea Warfare.

THIS PAGE INTENTIONALLY LEFT BLANK

TABLE OF CONTENTS

THIS PAGE INTENTIONALLY LEFT BLANK

LIST OF FIGURES

LIST OF TABLES

THIS PAGE INTENTIONALLY LEFT BLANK

LIST OF ACRONYMS AND ABBREVIATIONS

3D	Three-dimensional
DDES	Delayed Detached Eddy Simulation
IR	Infrared
LES	Large Eddy Simulation
ML	Mixed Layer
MLD	Mixed Layer Depth
NEQ	Non-Equilibrium
Q2D	Quasi-two-dimensional
SB	Submerged Body
SBD	Submerged Body Depth

THIS PAGE INTENTIONALLY LEFT BLANK

ACKNOWLEDGMENTS

First, I would like to thank my advisor, Timour, for making this achievement possible. Your passionate guidance has inspired many students. With your guidance, we can overcome any challenge.

It is difficult to express gratitude in words. Justin, thank you so much for always trying to make me understand and taking the time to tell me so much. Whatever path you want to take, I hope there will be no obstacles along the way.

I would also like to thank the faculty and staff at NPS. The effective teaching methods and conditions here have become the source of my academic achievement more easily. Thank you very much.

Finally, I want to thank my wife, Jaesil. You are brave, smart, sacrificial and stronger than anyone else. Thanks to your dedication, I have been able to achieve what I am today. I hope that everything we will be together in the future will be as happy as the present moment. I am happy to be able to share my dream with you.

THIS PAGE INTENTIONALLY LEFT BLANK

I. INTRODUCTION

A. MOTIVATION

Submarine detection is a critical component of anti-submarine warfare, but it faces challenges as the capacity for submarine concealment advances. With the development of submarine technology, including the reduction of propulsion engine noise and the reduced acoustic reflectivity of submarine hulls, submarines are becoming more difficult to detect using traditional acoustic methods.

One proposed alternative is the indirect detection of a submarine by the wake it generates. Objects traveling through fluid inevitably form wakes, which can produce detectable thermal and turbulent signatures at depth or at the sea-surface. Rather than requiring local instruments, surface signatures could potentially be identified remotely by aircraft or satellites, and this method of detection does not suffer from fundamental constraints that limit the applicability of acoustic-based algorithms.

A notable complication for surface detection in the ocean is the sub-surface mixed layer, which may affect the ability of a submerged wake to penetrate to the surface. Mixed layers, regions of 10–100 m in depth below the surface that are created and maintained by solar heating and wind forcing, are observed in all oceans. The mixed layer is characterized by almost uniform temperature and salinity. These regions often impede acoustic sensing of the environment by refracting sound waves towards the surface. This creates a shadow zone where surface detectors are blind to the presence of submerged objects. Thus, it is highly desirable to develop alternative detection techniques for submersibles propagating below the mixed layer. The ability of thermal and turbulent signals to penetrate this region is therefore a topic of immediate operational relevance.

B. BACKGROUND

The turbulent wakes in stratified fluids are traditionally described using the Froude number and the Reynolds number. The Froude number is a dimensionless number based on the stratification of the fluid

$$\mathrm{Fr} = \frac{U}{NL}, \tag{1.1}$$

where U is the velocity of the submerged body (SB) and L is the size of the SB. The buoyancy frequency (N) is

$$\mathrm{N} = \sqrt{\alpha g(\frac{\partial T}{\partial z})}, \tag{1.2}$$

where α is the thermal expansion coefficient, g is the acceleration due to gravity, $\frac{\partial T}{\partial z}$ is the vertical gradient of temperature. The Froude number is the ratio of the buoyancy and advective timescales. Low Froud number systems feel the impact of buoyancy strongly, and the wake flattens quickly. On the other hand, if the Froude number is large, the influence of buoyancy is negligible initially, and the influence of stratification is small. Generally, submarines have Froude numbers between 100 and 300. The Reynolds number is the ratio of inertial forces to viscous forces

$$\mathrm{Re} = \frac{UL}{\nu}, \tag{1.3}$$

where υ is the kinematic viscosity. Wakes produced by SBs are generally laminar when the Reynolds number is low (typically, ≤ 3000) and turbulent when it is high (≥ 5000). In general, submarines have large Reynolds numbers (10^8), and so, they generate strongly turbulent flows.

Prior work has led to insights into the evolution of the typical wake structure over time. Pao (1973) performed tank experiments with a towed grid and cylinder. He found that the mixing caused by the wake was substantial, enough to generate thermally homogenous regions. Subsequently, Spedding (1997) studied turbulent wakes in stably stratified fluids and identified their three distinct evolutionary stages: “near,” “intermediate,” and “far-field,.” Initially, turbulent wakes spread in three dimensions, unaffected by stratification. This effect was seen in Spedding (2002), who studied the vertical structure of a stratified wake in the immediate vicinity of the propagating object. This “near” or “three-dimensional” (3D)stage is followed by a non-equilibrium regime (NEQ). During the 3D stage, there is substantial vertical mixing that generates a conical homogenous region inside a stratified region. Because of buoyancy, the homogenous

region tends to settle at the level of neutral buoyancy, and the wake flattens. Some of the kinetic energy during the 3D stage is converted into potential energy and the rest maintains the wake turbulence. Once the NEQ regime starts, energy radiates away from the wake by internal waves, and this leads to the conversion of the stored potential energy into kinetic energy. At this stage, the collapse of the wake is observed. Lin and Veenhuizen (1974) performed laboratory experiments with grid-generated turbulence and observed that the vertical motion of turbulence in the stratification was reduced. The final stage is a quasi-two-dimensional (Q2D) state where the vertical motion is suppressed. Meunier and Spedding (2004) experimented with various objects, including cubes, cylinders, spheres, and ellipsoids, to determine the relationship between the shape of the object and the wake structure in a stratified fluid. They demonstrated that the wake structure does not significantly depend on the shape of the object.

The wake produced by an object in a stratified fluid can generate observable thermal and turbulent signatures. Voropayev, Nath, and Fernando (2012) conducted theoretical modeling and laboratory experiments to observe the wake generated by the movement of a ship. The wake caused by the movement of the scale model ship and propeller causes the rise of the cold seawater to the surface and thus the temperature difference can be detected via an IR camera. Lai, Moody, and Chakraborty (2017) performed direct numerical simulations (DNS) and confirmed that the detection is possible using thermal signatures on the surface. More recently, Radko and Lewis (2019) analyzed wake decay numerically and quantified the dissipation of turbulent kinetic energy and heat to analyze the rate of stratified decay, finding that local microstructure measurements could be used to recognize the presence of a wake hours after the passage of the body.

C. APPROACH

This study aims to determine how the presence of a mixed layer affects the surface signatures from a submerged propagating object. We perform a series of numerical experiments and vary the depth and velocity of the object, as well as the depth of the mixed layer. This study confirms that the submerged body produces a detectable thermal and velocity signal at the surface. In this study, we find that the mixed layer interferes with the

vertical spreading of the wake created by the SB and that deep mixed layers damp the signal.

This thesis is organized as follows. Chapter II explains the methodology and numerical experiments. Chapter III presents the simulation results. Finally, Chapter IV offers conclusions, describes the operational relevance of the study, and makes recommendations for future research.

II. METHODS

A. NUMERICAL MODEL

The following series of experiments represent a spherical submerged object transiting at a designated velocity (U) and depth (B) through a stratified fluid capped by a surface mixed layer. One of the key objectives is to investigate the effects of changing the mixed layer depth, M, on the resulting flow fields. The simulation configurations are summarized in Table 1.

Table 1. The summary of all experiments analyzed in this study

Case	M (m)	B (m)	U (m/s)
M0B10U5	**0**	**10**	**5**
M0B20U5	**0**	**20**	**5**
M0B40U5	**0**	**40**	**5**
M10B10U5	**10**	**10**	**5**
M10B20U5	**10**	**20**	**5**
M10B40U5	**10**	**40**	**5**
M20B10U5	**20**	**10**	**5**
M20B20U5	**20**	**20**	**5**
M20B40U5	**20**	**40**	**5**
M20B40U2.5	**20**	**40**	**2.5**
M20B40U10	**20**	**40**	**10**
M20B40U5	**20**	**40**	**5**
M20B40U5	**20**	**40**	**5**
M40B10U5	**40**	**10**	**5**
M40B20U5	**40**	**20**	**5**
M40B40U5	**40**	**40**	**5**

The simulations are performed using OpenFOAM (v2106), which is a finite volume code with unstructured meshing designed to allow for variable grid resolution near boundaries and subgrid-scale turbulence modeling. The unstructured mesh is ideal for simulating turbulent wakes. OpenFOAM has the capacity for dynamic meshing—in particular, a tool known as Overset (Tisovska 2019) —which permits the submerged object to be simulated in a mesh that travels with the object while the mesh containing the wake can be stationary. The overset technique couples these meshes by interpolation at the boundaries. The experiments performed fall in the category of Large Eddy Simulations

(LES), which numerically simulate turbulence occurring below the grid scale using additional equations that independently model the evolution of the turbulent kinetic energy and dissipation. The Spalart-Allmaras Delayed Detached Eddy Simulation (DDES) (Spalart et al. 2006) framework is used in this study, which evolves the turbulent viscosity as an additional field in the equations.

B. GOVERNING EQUATIONS

This following model is based on the Boussinesq approximation. The fluid is assumed to be incompressible (a good approximation for water), and its equation of state is characterized by linear relation between the density and temperature. We neglect the Coriolis force caused by the planetary rotation because the duration of the simulation is short compared to the rotational period of the Earth. The governing equations are the continuity equation, the linear equation of state, the temperature evolution equation and the momentum equation:

$$\nabla \cdot \mathbf{u} = 0, \tag{2.1}$$

$$\frac{\rho - \rho_0}{\rho_0} = -\alpha(T - T_{ref}), \tag{2.2}$$

$$\frac{\partial T}{\partial t} + \mathbf{u} \cdot \nabla T = (K_T + \nu_t/\mathrm{Pr}_t)\nabla^2 T, \tag{2.3}$$

$$\frac{\partial \boldsymbol{u}}{\partial t} + \mathbf{u} \cdot \nabla \mathbf{u} = -\frac{1}{\rho_0}\nabla p + g\alpha\big(T - T_{ref}\big)\hat{\mathbf{k}} + (\nu + \nu_t)\nabla^2 \mathbf{u}, \tag{2.4}$$

The symbol $\mathbf{u}$ represents the velocity vector, ρ is the density, $\rho_0 = 1024\ \mathrm{kg/m^3}$ is a reference density, $\alpha = 0.5\times10^{-4}\ ^{\circ}\mathrm{C}^{-1}$ is the thermal expansion coefficient, T is the sea-water temperature, and T_{ref} is a reference temperature. The symbol $K_T = 1.4\times10^{-7}\ \mathrm{m^2/s}$ represents the molecular diffusivity of heat, $\nu = 1\times10^{-6}\ \mathrm{m^{-2}s^{-1}}$ is the kinematic viscosity, and ν_t is the turbulent viscosity, which is determined by the turbulence model (the Spalart–Allmaras DDES). The symbol Pr_t represents the turbulent Prandtl number, which we assume to be 1 under the approximation that turbulence mixes temperature and velocity at the same rate (de Stadler 2010). The symbol p represents the pressure, $g = 9.81\ \mathrm{m/s^2}$ is the gravitational acceleration, and $\hat{\mathbf{k}}$ is the vertical unit vector.

C. EXPERIMENTAL CONFIGURATION

Figure 1 depicts the model setup. The entire computational grid contains two meshes. The "outer mesh" measures 700 m × 100 m × 270 m in the *x*, *y*, and *z* directions, respectively. The origin of the coordinate system is placed at the surface, 50m from the -*x* boundary and at the center of the domain in y. The body starts moving at (0, 0, -*B*) and ends at (600, 0, -*B*). The outer mesh has a resolution of 1 m. The upper boundary is impermeable and free-slip. The bottom boundary permits outflow, where fluid exiting the bottom has the normal gradients of *T* and **u** set to zero. The side, fore, and aft boundary conditions are periodic.

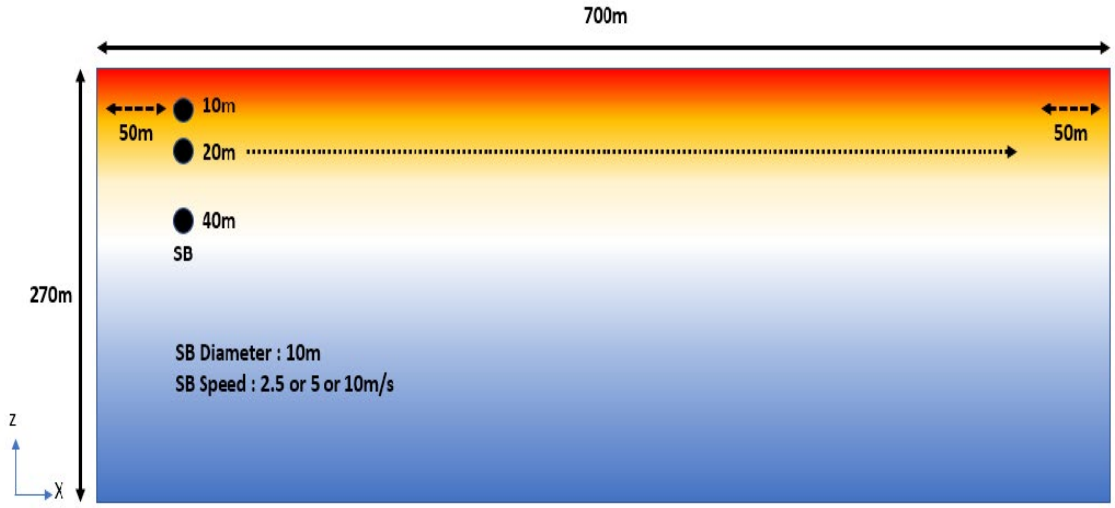

Figure 1. The schematic illustrating the model configuration. The *x*-*z* section is shown.

A separate "inner mesh" is introduced to represent the circulation in the vicinity of the moving object. This approach makes it possible to efficiently model the large-scale structures of the wake while concurrently resolving the boundary layer near the object. As depicted in Figure 2, the inner mesh is a cube with a size of 30 m, surrounding a 10-m-diameter submerged object. The inner mesh has variable resolution with an outermost resolution of 2 m, which becomes finer closer to the surface of the submerged object by refining the individual cells into octants. Each subdivision level is at least five cells wide.

The inner mesh is translated through the outer mesh to effectively represent the movement of the submerged object, and the temperature, velocity, and pressure at the outer edge of the inner mesh are interpolated from the outer mesh. The innermost 4 cm from the body boundary are meshed with cells normal to the face, creating five cell layers parallel to the body boundary with a finer variable thickness towards the boundary. The average thickness of cells at the borders of the body is 0.25 cm. This inner boundary is non-slip and impermeable, and the typical gradient of temperature and pressure on the surface is set to zero. The flow fields are interpolated from the inner mesh to the outer mesh just around the submerged body. When the submerged body depth (SBD) is 10 m (the M0B10U5, M10B10U5, M20B10U5, M40B10U5 cases), the upper part of the inner mesh rises above the water surface, so the height is adjusted from 30 m to 20 m as shown in Figure 3.

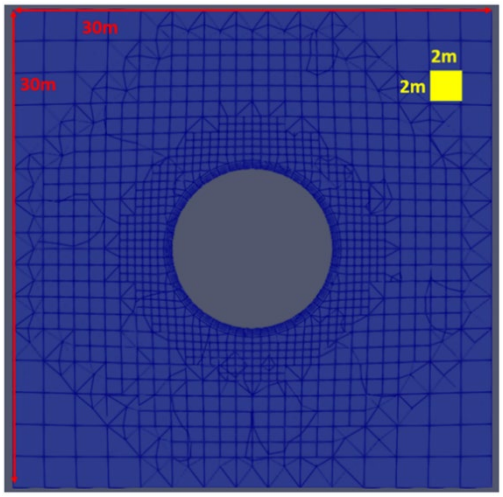

Figure 2. The vertical section of the inner mesh.

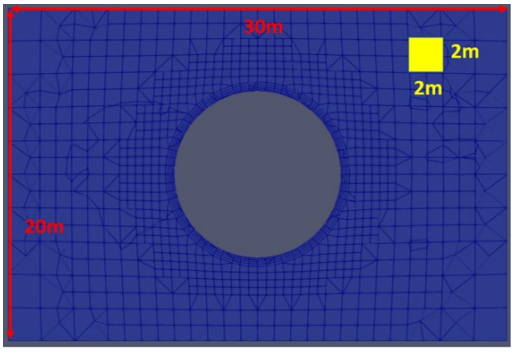

Figure 3. The vertical section of the inner mesh for cases with B=10 m.

To create the initial conditions for experiments, a mixed layer is created in a small periodic domain, which is tiled to fill the full simulation. The smaller domain permits the development of the mixed layer over an extended period at reduced computational cost. This initial mesh for these setup simulations is 100 m × 100 m × 180 m in size with a resolution of 1 m. The boundary conditions are the same as the experimental mesh except on the surface, where wind forcing is used to generate a mixed layer. At the surface, the velocity is set to

$$\mathbf{u} = (W\cos(tf), 0, 0), \tag{2.5}$$

where W is the amplitude and f is the frequency of the wind oscillation. The amplitude and frequency are varied to generate a desired mixed layer depth, as shown in Table 2. These simulations are initialized with a uniform temperature gradient of 0.05 ℃/m

Table 2. Wind stress characteristics used to create a ML of desired depth

***M* (m)**	**Amplitude**	**Frequency (Hz)**
10	**0.15**	**0.01**
20	**0.2**	**0.01**
40	**0.1**	**1**

The final temperature profile of the setup simulation is shown in Figure 4, which shows uniform stratification in the mixed layer and uniform stratification below. After the

setup simulation has run for one week of simulated time, we tile the final three-dimensional output in x and y to fill the outer mesh as the initial condition (as illustrated in Figure 5). The region of z < -180 m is initialized with a uniform gradient in temperature and no initial velocity. Because the surface velocity of the wake is a quantity of interest, the surface of the outer mesh uses a free-slip boundary. This has the consequence that the mixed layer is no longer being forced and will eventually decay. However, we demonstrate that the decay timescale is longer than the duration of our simulations by measuring the turbulent dissipation rate. The turbulent dissipation rate is the rate by which turbulent kinetic energy is converted into thermal energy and is given by

$$\varepsilon = \sqrt{fv_1} \times (C_\mu k)^2 / \tilde{v}, \tag{2.5}$$

where $k = (\sqrt[3]{f_{v1}} \times \tilde{v} \times \sqrt{2/C_\mu} \times |grad\ U|)$, $\tilde{v} = v_t / f_{v1}$, $fv_1 = \chi^3 / (\chi^3 + {C_{v1}}^3)$, $\chi = \tilde{v} / v$, $C_\mu = 0.09$, $C_{v1} = 7.1$. We plot the maximum turbulent dissipation rate in Figure 6, which shows that the decay time of the mixed layer in the absence of external forcing is approximately 7 hours, much longer than our simulations.

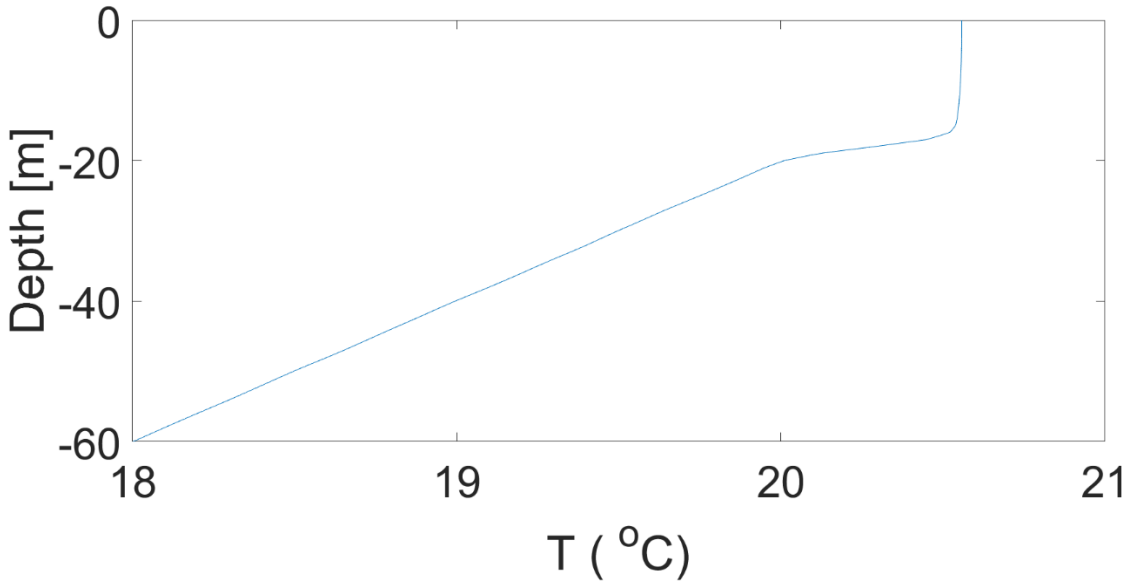

Figure 4. Initial temperature profile.

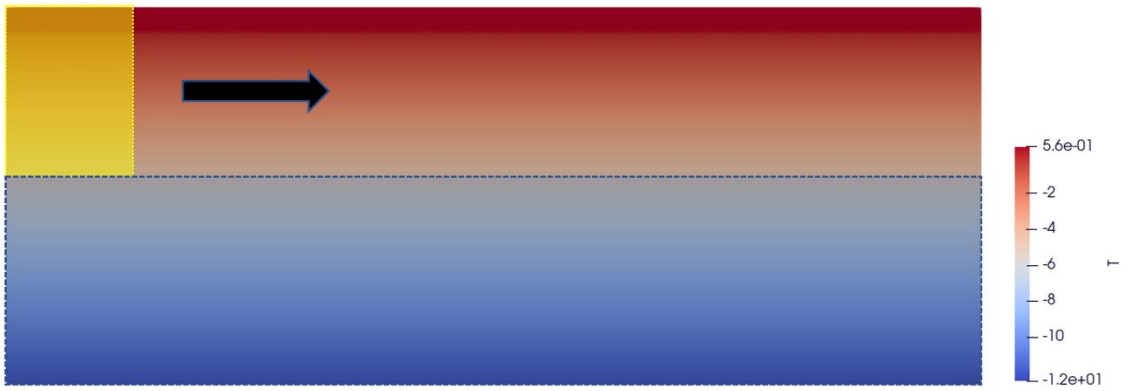

Figure 5. Mesh creation through tiling of the preliminary mixed-layer simulations.

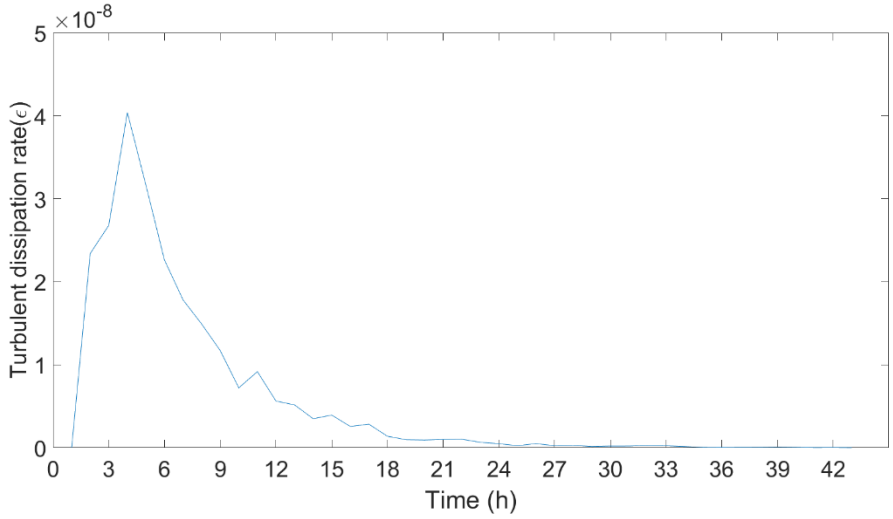

Figure 6. The turbulent dissipation rate over time in the simulation.

We perform a resolution test to check the convergence of the turbulence model in Figure 7. This involves two simulations with identical domain sizes but with one simulation having 50% more cells in each dimension. In these simulations, the body is towed through the domain with $M = 20$ m, $B = 20$ m, $U = 5$ m/s. We display the evolution of the maximum turbulent dissipation rate in Figure 7. The turbulent dissipation rates are comparable between the two simulations, showing similar magnitudes and variability.

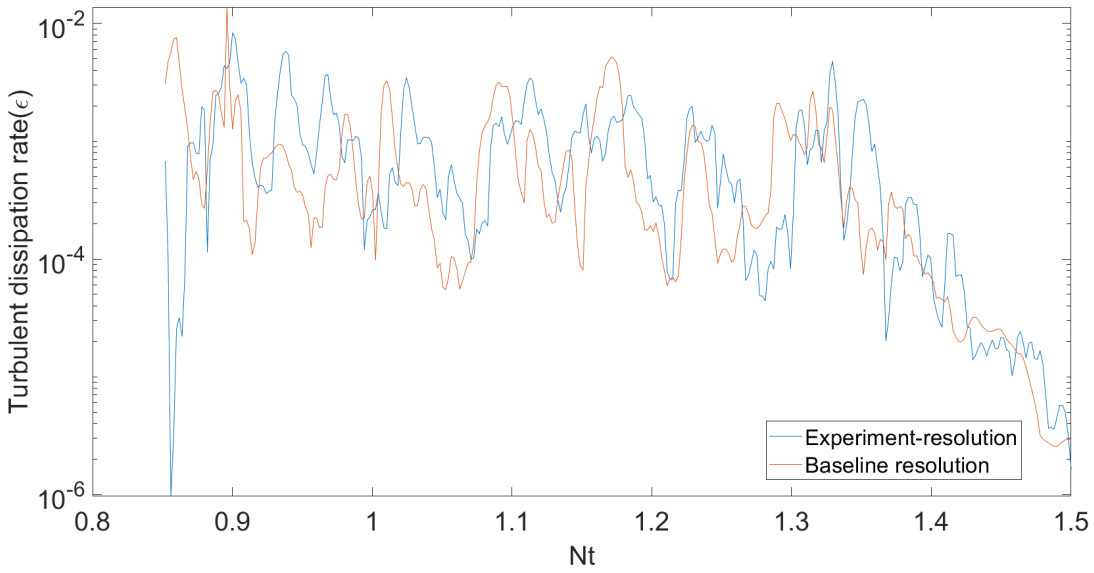

Figure 7. Comparison of the turbulent dissipation rates in two simulations with different resolution.

III. RESULTS

A. PHENOMENOLOGY

The typical evolution of one of these wake simulations is shown in Figure 8, which shows the velocity cross-section in the Y direction at 200 seconds after the SB starts moving. The experimental parameters are M = 20 m, B = 40 m, and U = 5 m/s. As the SB propagates, it creates turbulence, which spreads horizontally and vertically. The horizontal motion adds momentum to the fluid, as seen on the right side of the figure. Some of the velocity perturbations appear in the form of a plume or extend to the surface. The region on the left that doesn't appear turbulent is a "startup transient" which occurs because the fluid is initially at rest, and it only becomes turbulent after a finite period. Even after the SB passes, the wake maintains mean flow, while the surface temperature and velocity change.

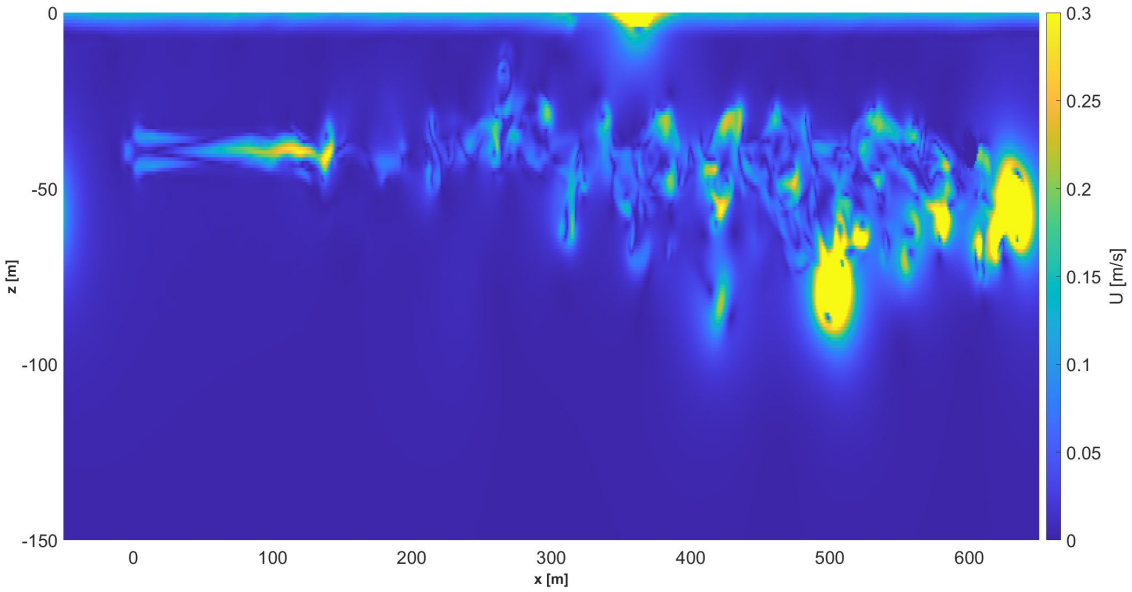

Figure 8. The x-z section of absolute velocity for the M20B40U5 case at t = 200s.

We illustrate the observable sea-surface signature for this simulation in Figure 9. We express the thermal signal in terms of the temperature perturbation ΔT:

$$\Delta T = T - T_0, \tag{3.1}$$

where T_0 is the initial temperature prior to the generation of the turbulent wake. 200 seconds after the body has passed, relatively cold water-masses initially located below the mixed layer rise to the sea-surface. The surface pattern is characterized by the emergence of thin streams and vortices. The upward displacement of fluid from the depth of 40 m to the surface is due to the turbulent wake created by the SB. The upwelling of cold fluid is particularly intense during the first, thee-dimensional stage of wake development. These cold surface temperature anomalies disperse over time as they are dissipated by turbulence and diffusion, eventually becoming undetectable. However, as shown in the bottom panel of Figure 9, they are easily observable even after 1,000 seconds.

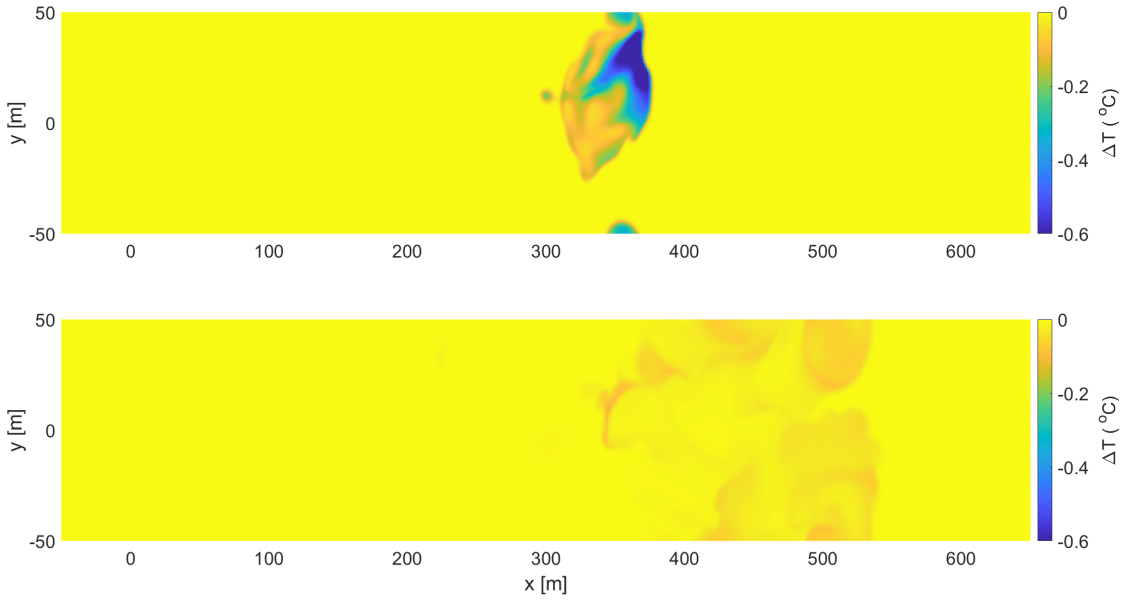

Figure 9. The temperature field at the sea-surface for M20B40U5 case. The upper panel shows the surface at *t*=200 s, and the lower panel, at *t*=1,000 s

Another observable surface wake signature is the velocity at the sea-surface, which can be substantial. We plot the magnitude of the lateral surface velocity in Figure 10. The

wake generated by the SB moves in the horizontal and vertical directions, and in the region where these movements are applied, a faster speed than the surrounding is observed. The morphology of the velocity field at the surface is comparable to the temperature perturbation shown in Figure 9, and it dissipates gradually in a similar manner. At 200 seconds, the velocity in the turbulent wake greatly exceeds that of the mixed layer.

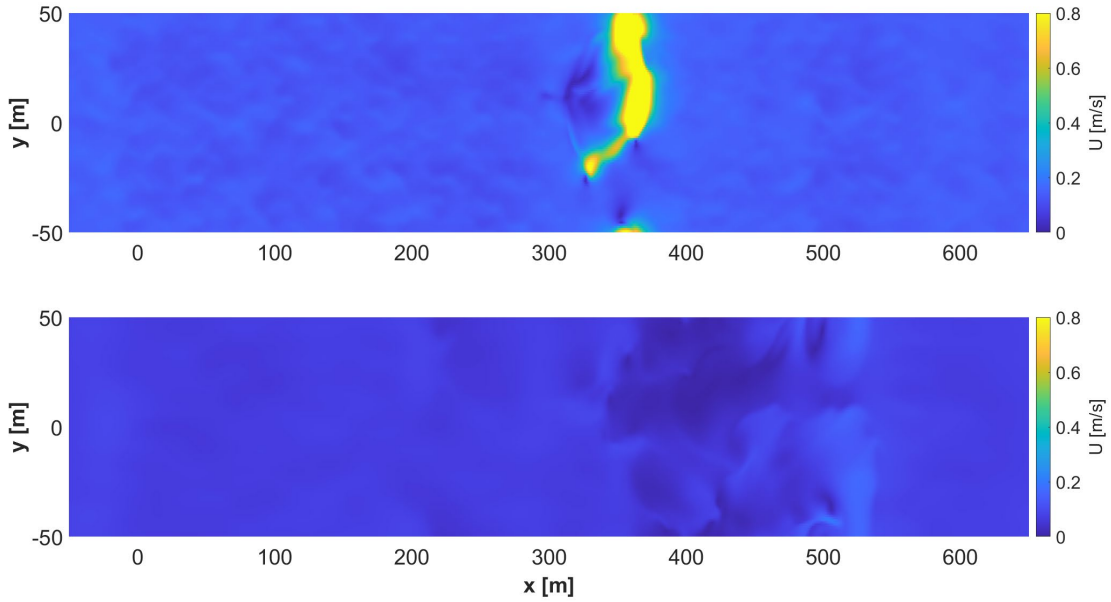

Figure 10. The velocity field at the surface for the simulation in Figure 9.

B. EFFECTS OF THE VARIATION IN MLD

Figure 11 and Figure 12 explore how the presence of a mixed layer affects the thermal surface signal. For B = 40 m and U = 5 m/s, a case without a mixed layer and a case with M = 20 m were compared. In the absence of the ML, a larger and stronger signal appears, and it persists after 3,000 seconds. In contrast, when the ML is present, the signal is much weaker and only lasts for 2,000 seconds. This demonstrates that the ML inhibits the vertical expansion of the wake.

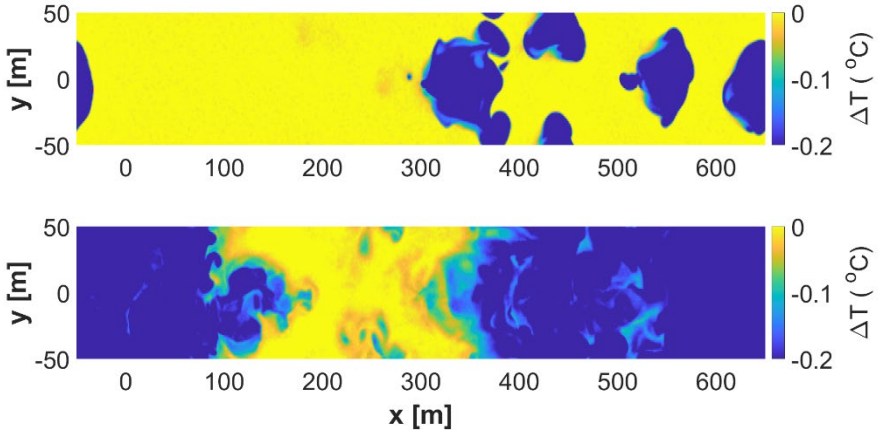

Figure 11. The temperature field at the surface for the M0B40U5N2 case at t = 300 s (top panel) and t = 3,000 s (bottom).

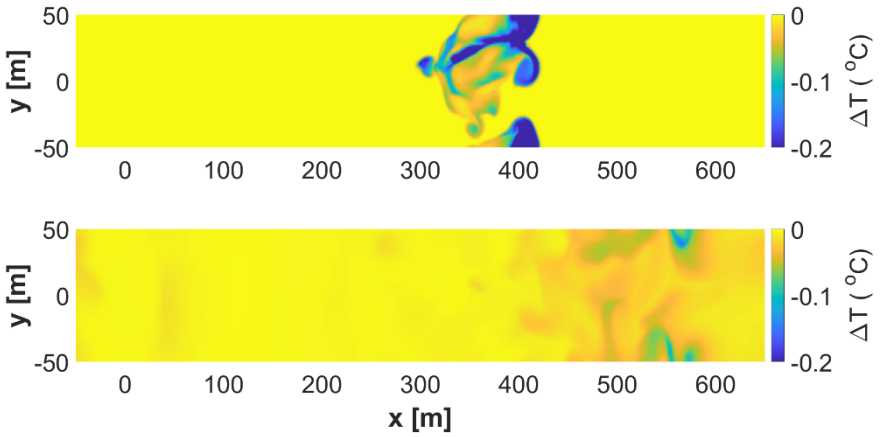

Figure 12. The temperature field at the surface for the M20B40U5N2 case at t = 300 s (top) and t = 3,000 s (bottom).

Figure 13 presents the temperature change at the surface for simulations with varying M and with B = 40m. It expresses the average (ΔT_{avg}) and the maximum (ΔT_{max}) values of the temperature anomaly as a function of time. As the MLD increases, the amplitude of the temperature signal monotonically decreases. The initial temperature signal occurs as the wake breaks through to the surface and then decreases gradually as turbulence and diffusion dissipate the temperature. Simulations with shallower ML show stronger temperature anomalies, consistent with our prior argument. Typical surface perturbations are 0.47° C without a mixed layer, but this can decrease to 0.37° C for a

mixed layer depth of 10 m, 0.21° C for 20 m, and 0.03° C for 40 m. The strongest local features in the surface temperature can be four times as intense. This suggests that the presence of an ML inhibits the detection of submarine wakes.

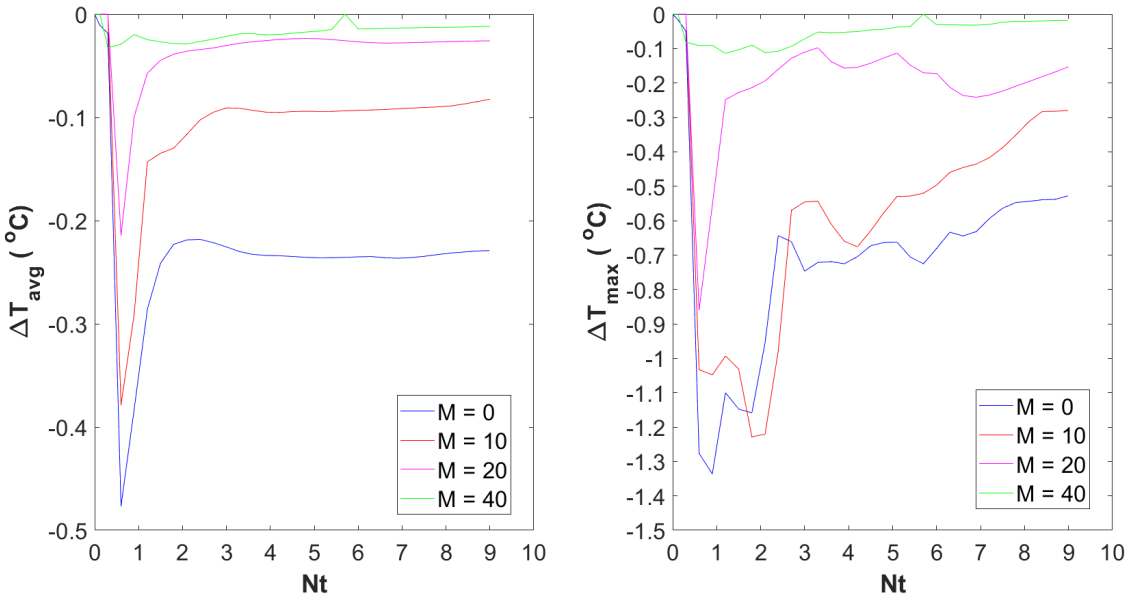

Figure 13. The average and maximum temperature field at the surface as a function of time for various values of M. The left panel presents the average temperature anomaly in the region affected by the wake. The right panel is the maximum anomaly in the same region.

Figure 14 shows the area affected by the wake as a function of time. The area is calculated as follows:

$$A_T = \int\int \Theta(|T - T_0| - T_{threshold})\mathrm{dxdy} \tag{3.2}$$

where Θ is the Heaviside function and $T_{threshold} = 0.01$ ºC is a threshold temperature. We use a threshold of 0.01 ºC, which is comparable to the precision of airborne infrared (IR) cameras (Zappa 2005). At the stage when turbulence is formed, the area of the affected surface increases rapidly. Thereafter, the area affected by the wake gradually decreases. In the absence of a mixed layer, turbulence is more vigorous and its onset is more rapid. Also, the elevated temperature signal lasts longer. On the other hand, when a mixed layer is present, surface signatures are more limited. As the MLD decreases, the wake affects a

larger area of the surface. This substantially improves the capacity to detect surface features as the features are both larger and exhibit more extreme temperatures.

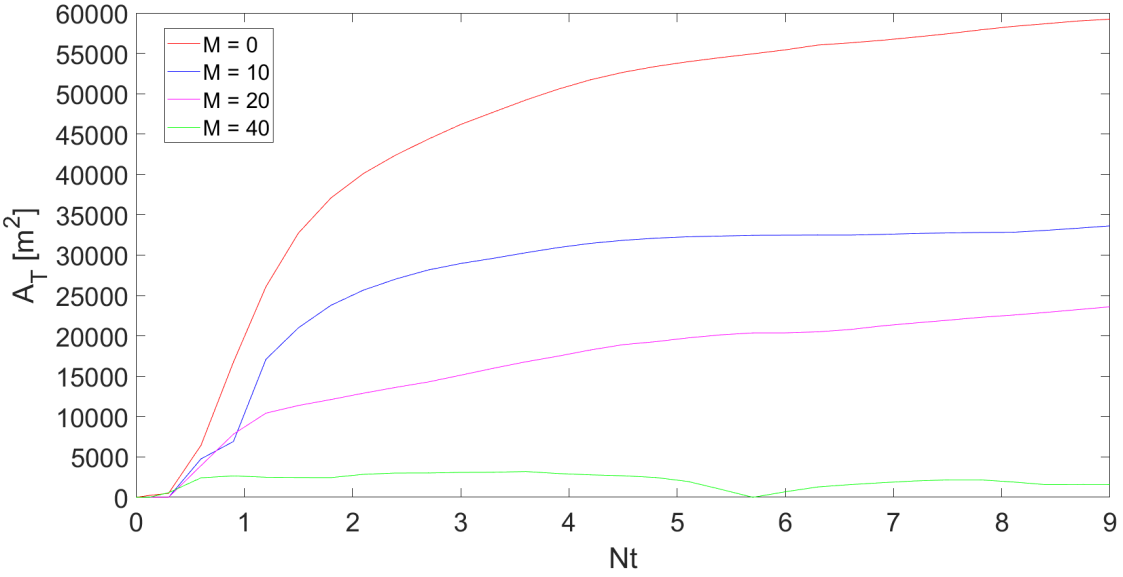

Figure 14. The area of the temperature perturbation over time for the simulations in Figure 13.

This weakening of the thermal signature with deeper mixed layers is also apparent in simulations performed with B=20 m, which are shown in Figures 15 and 16. As in the case of B = 40 m, the surface temperature anomaly weakens as the depth of the mixed layer increases. Of note, for M = 40 m, the SB is entirely embedded within the mixed layer, which results in a negligible difference between the temperature of the active water depth and the surface. Therefore, in simulation M40B20, there is almost no change in the surface temperature signal due to the wake. The observation of these temperature fluctuations appears similarly to the B = 10 m case. The effect is also supported by diagnostics is in Figures 17 and 18. In conclusion, MLD affects turbulence generated by SB for all values of B considered in this study.

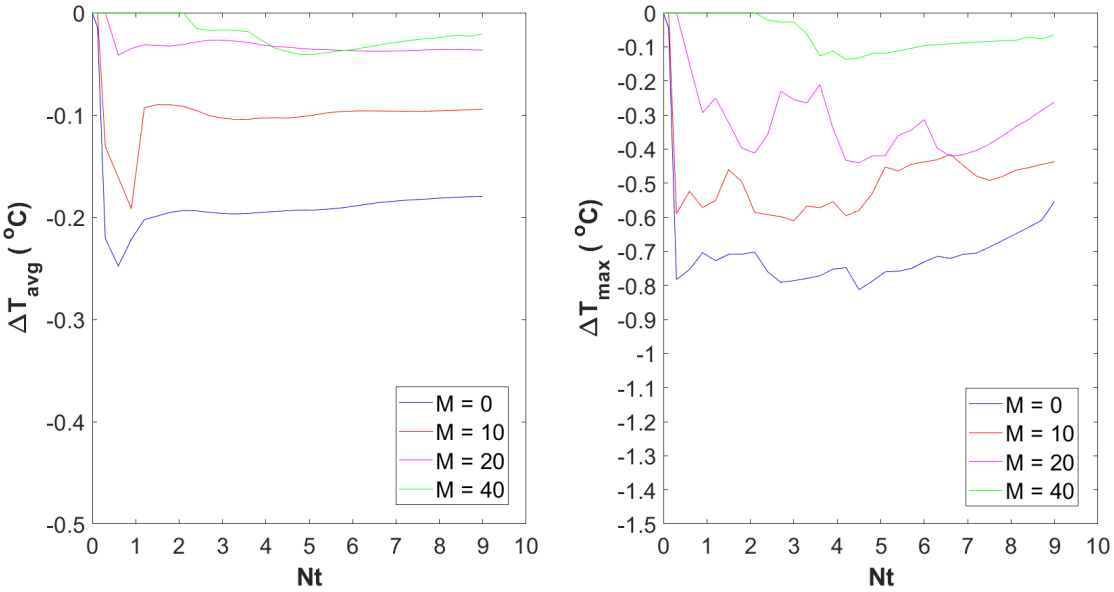

Figure 15. The average and maximum temperature anomalies at the surface for various values of MLD and B = 20 m.

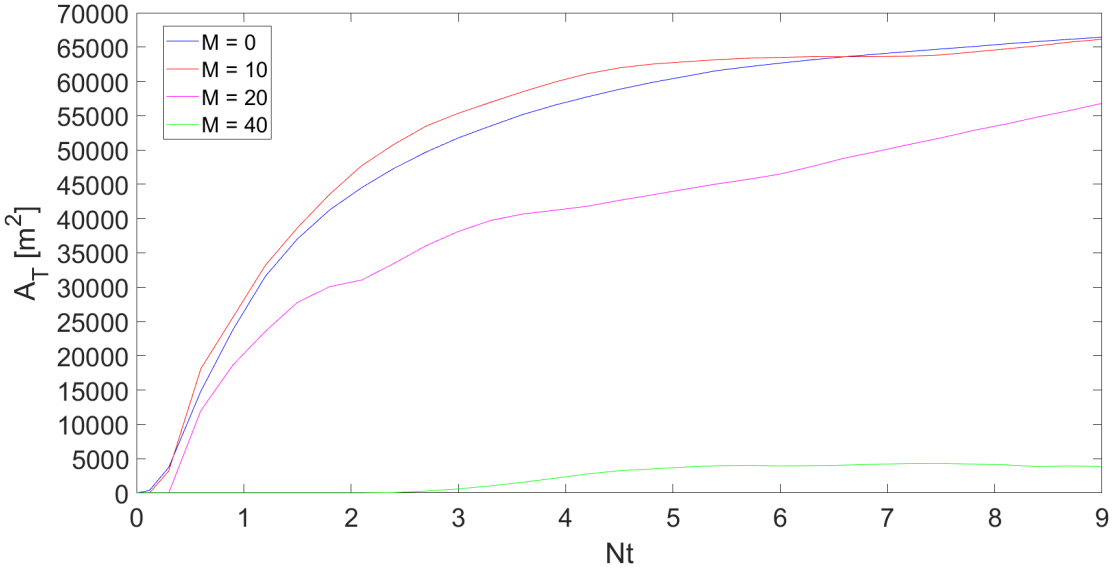

Figure 16. The area of the temperature perturbation over time for the same case depicted in Figure 15.

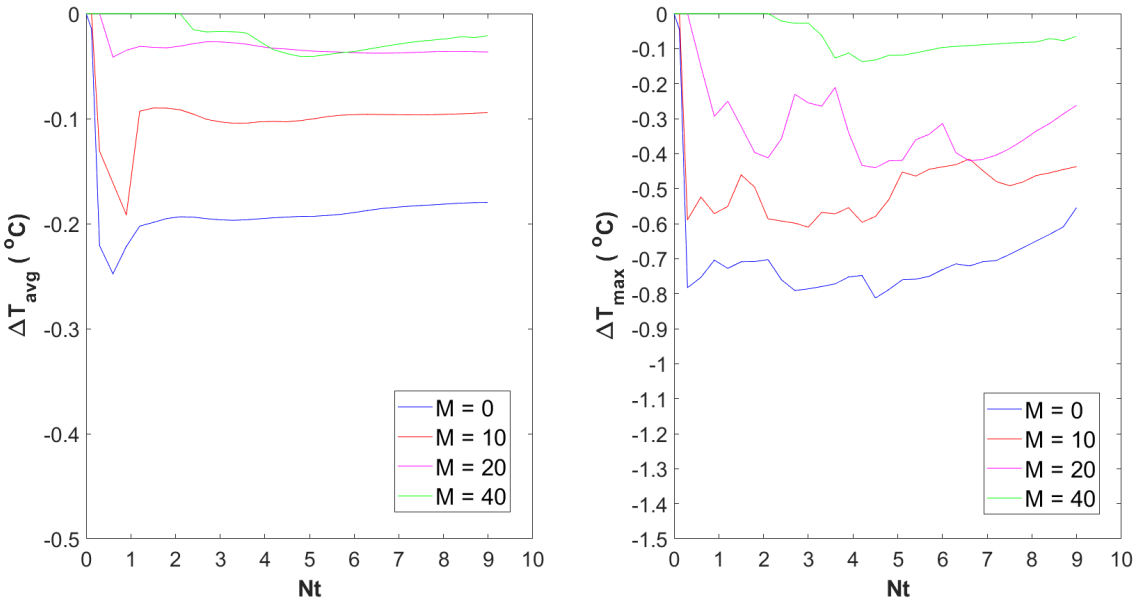

Figure 17. The average and maximum change of temperature field at the surface for according to the MLD change for B = 10 m.

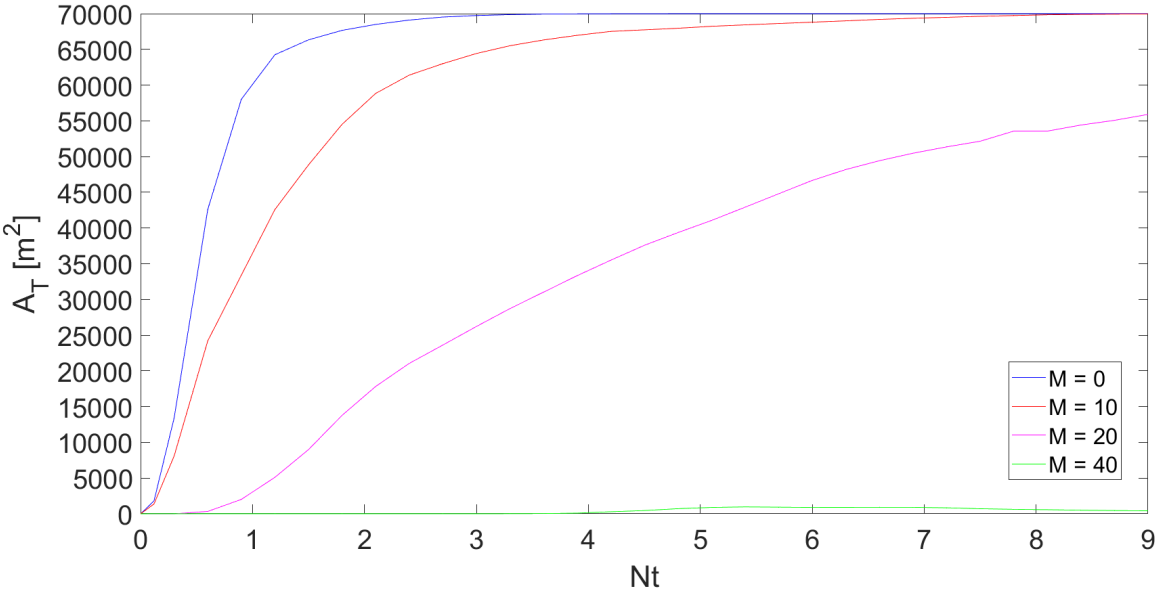

Figure 18. The area of the temperature perturbation over time for the simulations in Figure 17.

C. EFFECTS OF THE VARIATION IN THE SPEED AND DEPTH OF THE SUBMERGED OBJECT

Figures 18 and 19 show the surface temperature signal for simulations with SB speeds of 2.5 m/s, 5 m/s, and 10 m/s. In all simulations, M = 20 m and B = 40 m. To compare wake patterns realized at the same evolutionary stages, the surface temperature was recorded when a similar amount of time elapsed after the SB arrived at the stopping point. In the slower velocity case, the SB arrives at the target point after 280 seconds; so, 280 seconds is set as the reference time.

$$Ns = N \times (t - 280). \tag{3.3}$$

In the U=5m/s case, the SB arrives at the target point after 140 seconds; thus, 140 seconds is set as the reference time,

$$Ns = N \times (t - 140). \tag{3.4}$$

Likewise, in the U=10m/s case,

$$Ns = N \times (t - 70). \tag{3.5}$$

Therefore, the time specified on the x-axis of the graphs (Figs. 19, 29) is expressed in terms of Ns.

Figure 19 indicates that the temperature change due to turbulence has a greater effect in the case of high speed than in the case of slow speed. More turbulence leads to more mixing and larger wakes. More mixing and larger wakes, in turn, lead to broader surface patterns. We note that the size of the affected area increases almost monotonically in time in the case with the slow speed, but in the high-speed experiment, the area expands violently at the initial stage. The higher the speed, the higher the Reynolds number, the more turbulent the wake, and the faster it expands. Therefore, when the submarine moves rapidly, the signal is expected to be transmitted quickly toward the sea-surface.

As can be seen in Figure 20, a strong signal was generated first in the cases with higher speed compared to the case of U=2.5. In the case of U=2.5, the strong signal was transmitted to the surface relatively late. Overall, the average temperature change occurred up to 0.4° C in the U=2.5 m/s case, while the U=5 m/s case and U=10 m/s case had a change

of about half of that. However, in terms of maximum temperature change, by contrast, the case with the high speed reaches a change of about 1 ° C, and the case with the slow speed changed up to about 0.8 ° C. Thus, if SB is moving fast, a strong signal tends to be concentrated, and if SB is slow, the signal tends to spread.

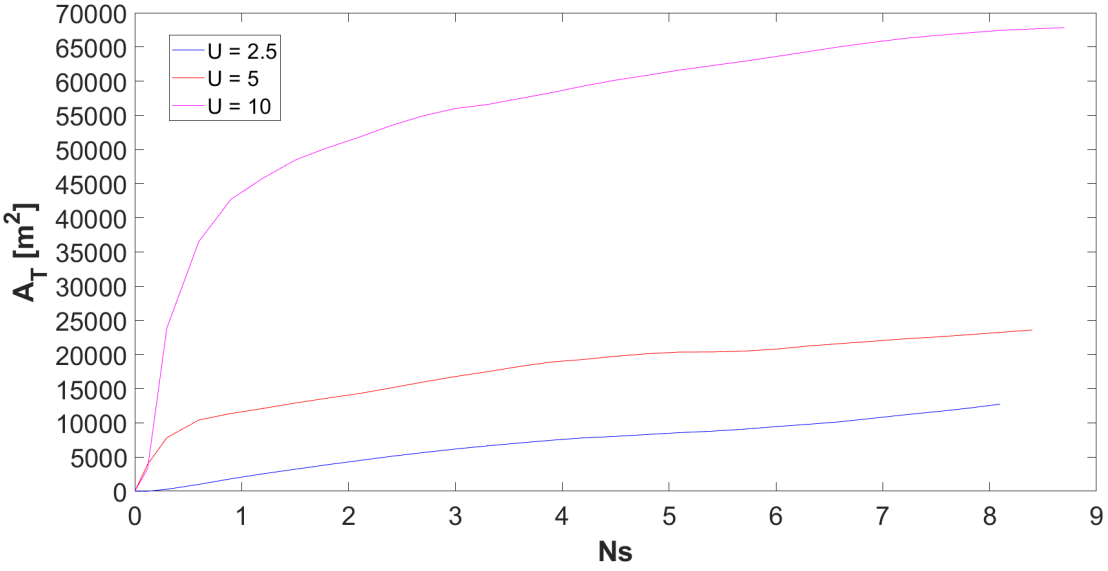

Figure 19. The area of the temperature perturbation as a function of time for M = 20 m, B = 40 m. Red, blue, and purple curves represent simulations with U=2.5 m/s, U=5 m/s, and U=10 m/s, respectively.

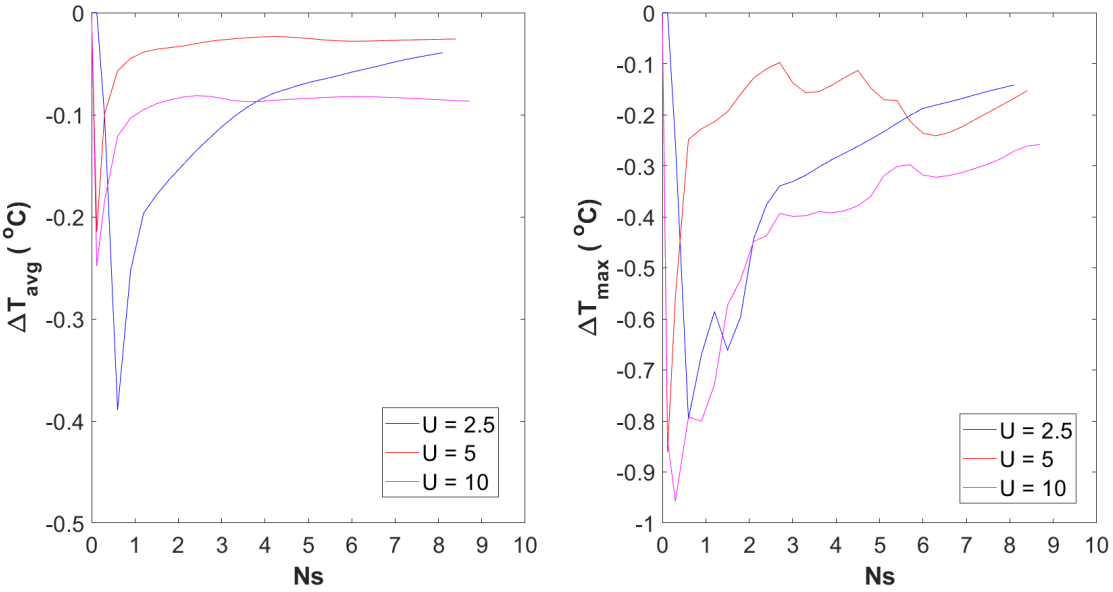

Figure 20. The average and the maximum values of the temperature change in the region affected by the wake for the simulation in Figure 18. Red, blue, and purple curves represent U=2.5 m/s U=5 m/s, and U=10m/s, respectively.

Figure 21 shows the surface temperature signal for simulations with B = 10 m, 20 m, and 40 m, respectively. All simulations were performed with M = 10 m and U = 5 m/s. As the depth of the SB increases, the surface temperature perturbation increases, and the size of the region where these changes occur decreases. The magnitude of the thermal surface signal correlates with the difference between the surface temperature and the temperature at the body depth. The surface temperature change between the B = 10 m and 20 m cases in the mixed layer was not significantly different, but the B = 40 m case (in which the submersible moves below the mixed layer) exhibited a temperature anomaly about twice as large as in the 10 m and 20 m cases. The intensification of the signal for B = 40 m is attributed to the direct displacement of cold seawater below the mixed layer by the wake. Therefore, the attempts of an adversarial submarine to avoid acoustic detection by operating the shadow zone in the lower part of the mixed layer could be countered by wake-detection methods. In such conditions, strong temperature signal reaches the surface due to the turbulence.

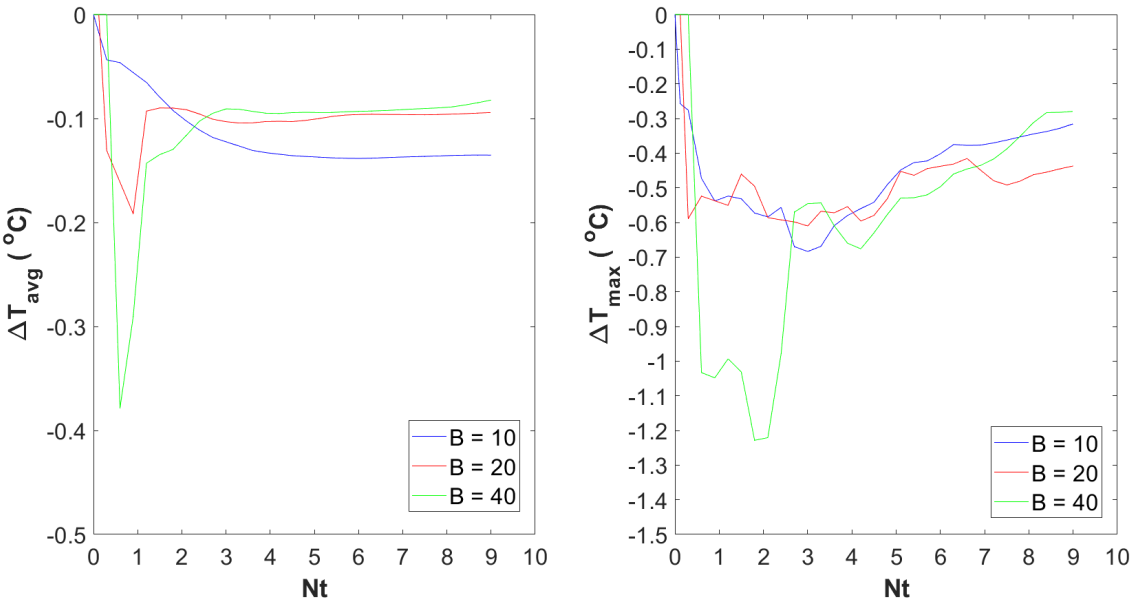

Figure 21. The average (left panel) and maximum (right panel) surface temperature anomaly plotted as a function of time for M = 10 m and various values of B. Blue, red, and green curves represent simulations with B = 10 m, B = 20 m, and B = 40 m, respectively.

Figure 22 shows the area of large surface temperature anomalies (A_T) as a function of time for various values of B. The temporal patterns of A_T for different values of B are similar. However, in the case of B = 10 m, the surface area subtended by the wake is larger. Since in this case SB is close to the surface, it can affect the large region due to the horizontal and vertical motion of the wake. On the other hand, in the case of B = 40 m, it affects a narrower area. This trend is similar to the case of M = 20 m shown in Figures 23 and 24. As previously argued, as the MLD increases, the surface temperature signal weakens. The case of M = 40 m exhibited a weaker variation in temperature anomalies than other simulations. This is attributed to the lack of variation in temperature at the cruising depth of SB.

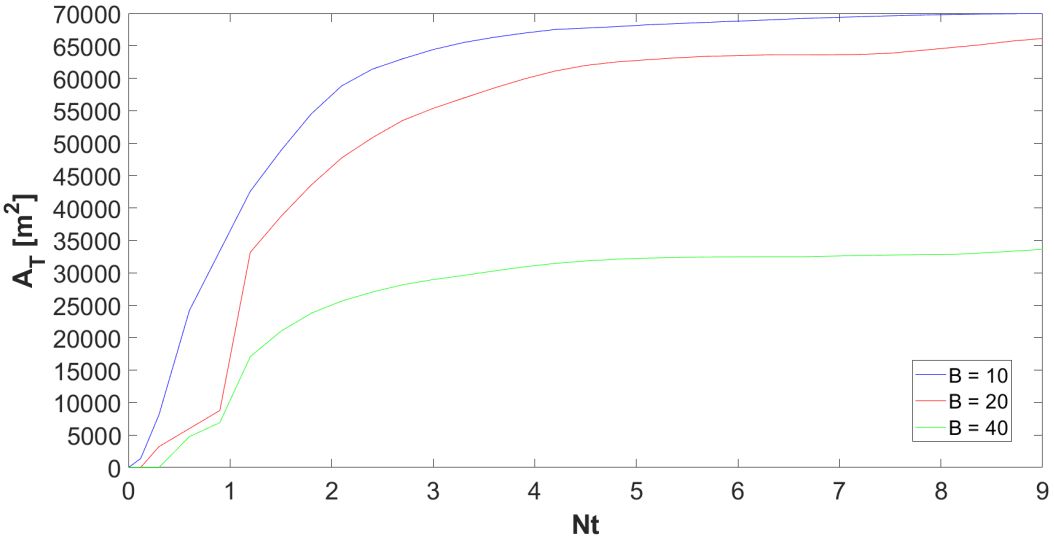

Figure 22. The area of the temperature perturbation for the simulation in Figure 17. Blue, red, and green curves represent B=10 m, B =20 m, and B =40 m, respectively.

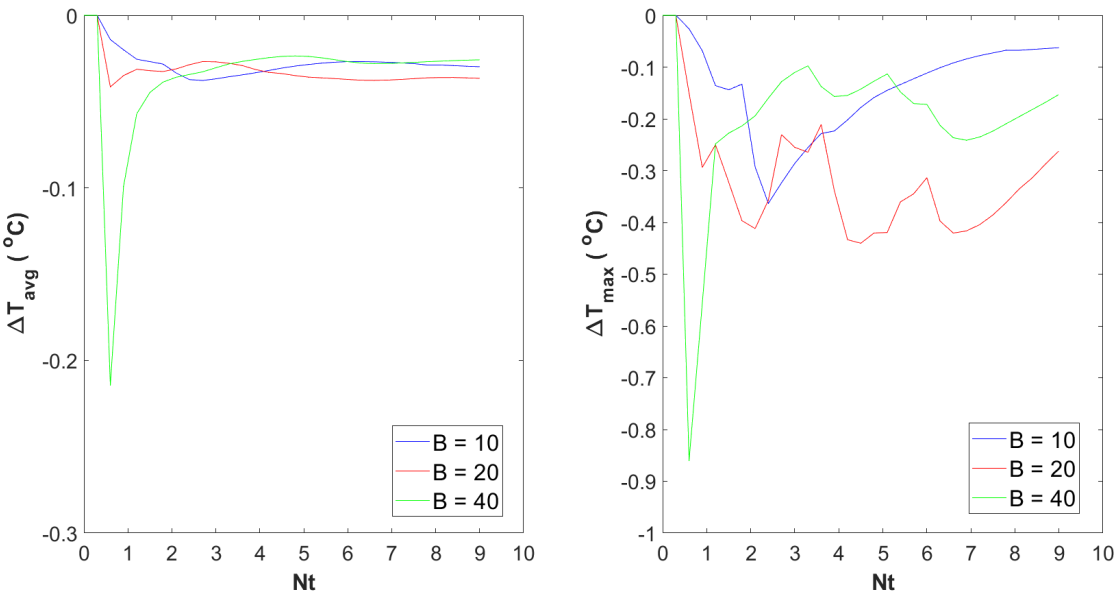

Figure 23. The average (left) and maximum (right) surface temperature anomalies as a function of time for M = 20 m and various values of B.

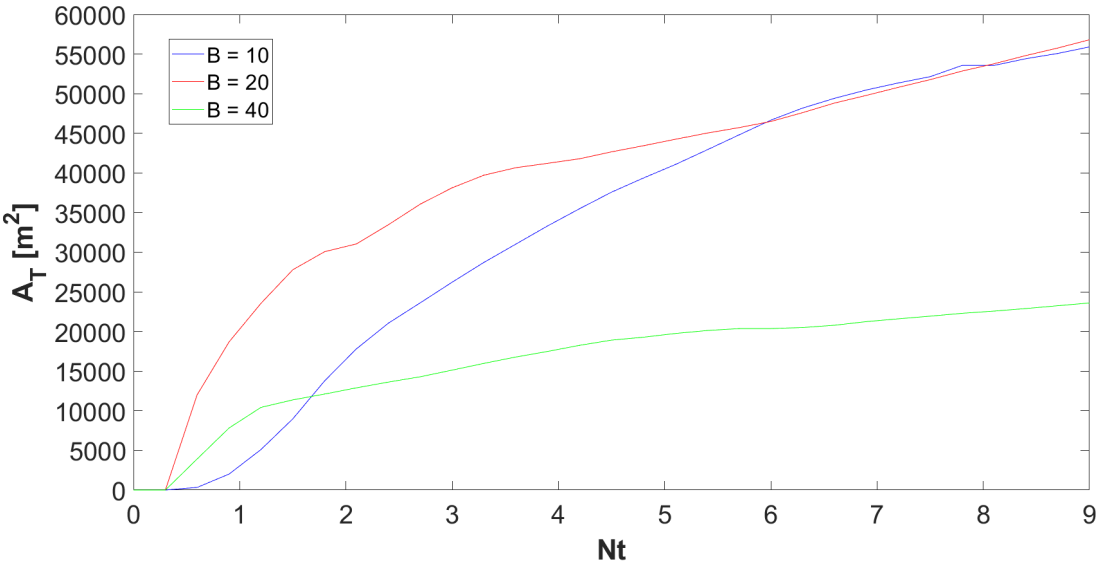

Figure 24. The area of the temperature perturbation as a function of time for the simulation in Figure 23.

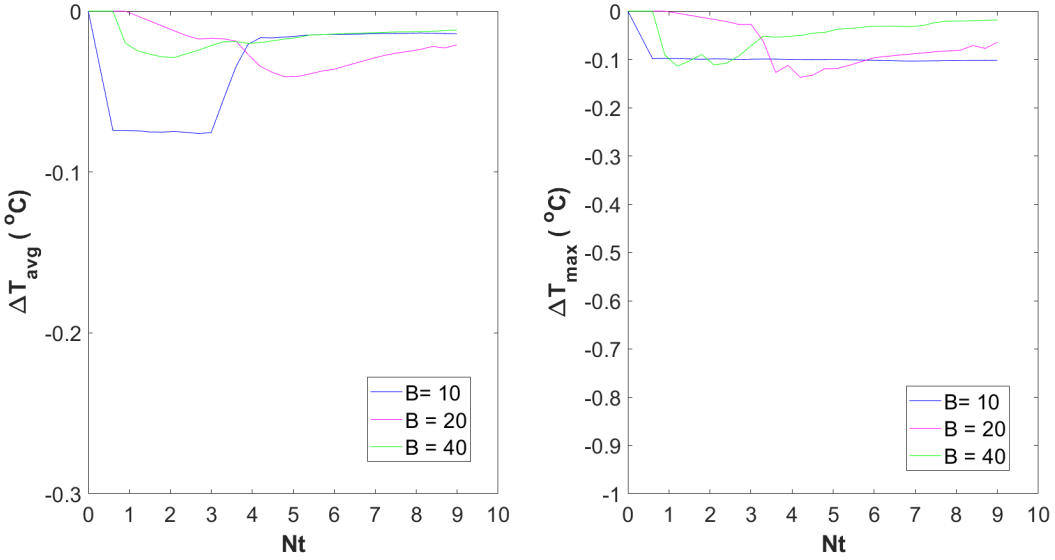

Figure 25. The average (left) and maximum (right) surface temperature anomalies as a function of time for $M = 40$ m and various values of B.

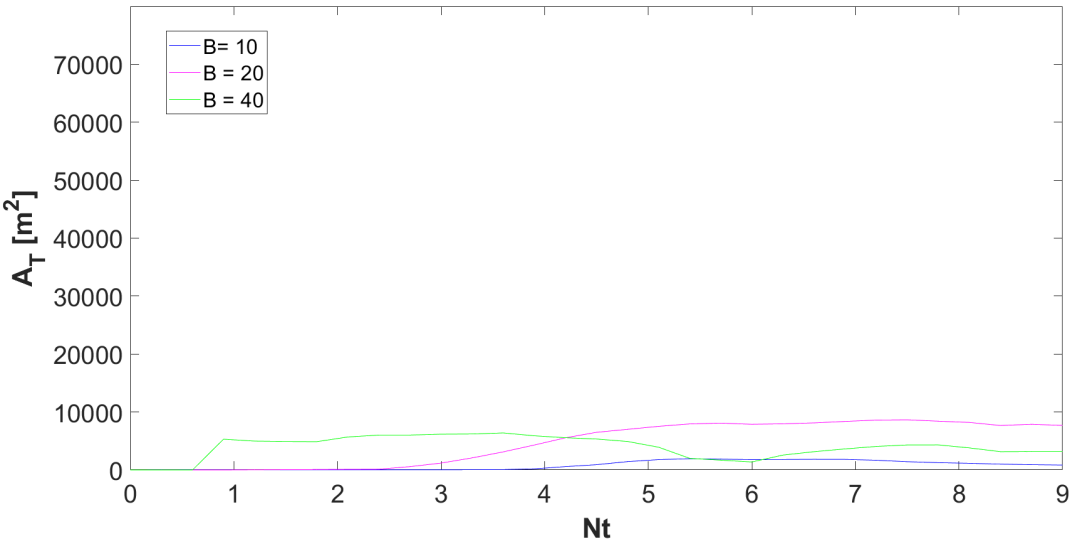

Figure 26. The area of the temperature perturbation as a function of time for the simulation in Figure 25.

THIS PAGE INTENTIONALLY LEFT BLANK

IV. DISCUSSION

In this study, wake simulations were performed in the presence of a mixed layer. The key objective of this effort was to determine whether and how the thermal and velocity perturbations generated by propagating submersibles can reach the sea-surface. Based on a series of high-resolution experiments, we conclude that deeper mixed layers led to weaker surface signatures. This occurs because deeper mixed layers (for the same sub-mixed-layer stratification) imply weaker temperature variation between the surface and the depth of the submerged body. Faster SBs are shown to produce much larger surface regions with detectable thermal anomalies. The signal strength is less sensitive to the depth of the propagating object. Initially, deep-moving submersibles exhibit stronger surface perturbations than their shallow counterparts. However, this trend reverses at the later stages of wake evolution.

Submarine detection is a critical component of Undersea Warfare (USW). The mixed layer is present in most of the World Ocean and therefore our ability to detect and interpret the signatures of moving submersibles transmitted through the mixed layer to the sea-surface can greatly enhance the effectiveness of anti-submarine operations. The sea-surface temperature anomalies predicted by this study range from -0.1 °C to -1.4°C, affecting the areas from 5,000 m^2 to 60,000 m^2. Given the capability of an aircraft's IR camera to distinguish between 0.02° C of temperature change or less and within 1 m or less, the signal is clearly detectable (Zappa 2005). Based on our experiments, we expect detectable signals to last for at least 1,000 seconds or more. Such signal duration is expected provide enough time for reliable detection in naval operations. Overall, we anticipate that detecting surface signals will complement the conventional methods, particularly if environmental conditions restrict the acoustic sensing of submersibles.

Although this work demonstrates the feasibility of identifying submerged bodies by their surface hydrodynamic signatures, further research is needed. The importance of environmental factors, such as continuous wind forcing, surface and internal waves, surface heating/cooling and evaporation/precipitation should be considered. In addition, it is desirable to validate the presented numerical inferences using the corresponding field

and laboratory experiments. In addition, the present investigation must be expanded to include a wider range of spatial and temporal scales. It is important to trace the surface signal over more extended periods and thereby determine how long it takes for the signal to disappear completely.

LIST OF REFERENCES

Brucker Kyle A., & Sarkar Sutanu, 2010: A comparative study of self-propelled and towed wakes in a stratified fluid, *Journal of Fluid Mechanics*, **652**, 373–404, https://doi.org/10.1017/S0022112010000236.

Cheng Li, Cheng, L., Zhu, J., Trenberth, K. E., Mann, M. E., & Abraham, J. P. ,2020: Increasing ocean stratification over the past half-century. *Nature Climate Change*, **10**, 1116–U76. https://doi.org/10.1038/s41558-020-00918-2.

Diamessis Peter J., Spedding G. R., and Andrzej Domaradzki J. (2011). *Similarity scaling and vorticity structure in high-Reynolds-number stably stratified turbulent wakes*. Cambridge University Press.

de Stadler, M. B., S. Sarkar, and K. A. Brucker, 2010: Effect of the Prandtl number on a stratified turbulent wake. *Physics of Fluids*, **22**, 095102–095102–15, https://doi.org/10.1063/1.3478841.

Lin J. T., & Pao Y. H. 1974: *Turbulent wake of a self-propelled slender body in stratified and non-stratified fluids: Analysis and flow visualization*. APL/JHU POR-3586.

Lai, J., A. Moody, N. Chakraborty, 2017: Turbulent kinetic energy transport in head-on quenching of turbulent premixed flames in the context of Reynolds Averaged Navier Stokes simulations. *Fuel*, **199**, 456–477.

Lin, J. T., & Pao Y. H., 1979: Wakes in stratified fluids. *Annu. Rev. Fluid Mech*., **11**, 317–338., https://doi.org/10.1146/annurev.fl.11.010179.001533.

Mellor, G. L., Durbin, P. A. 1975: The structure and dynamics of the ocean surface mixed layer*, Journal of Physical Oceanography*, **5**, 718–728 https://doi.org/ 10.1175/1520-0485(1975)005<0718:TSADOT>2.0.CO;2.

Meunier, P., & Spedding, G. R., 2004: A loss of memory in stratified momentum wakes. *Physics of Fluids*, **16**, 298–305, https://doi.org/10.1063/1.1630053.

Moody, Z. E., C.J. Merriam, T. Radko, and J. Joseph, 2017: On the structure and dynamics of stratified wakes generated by submerged propagating objects. *J. Oper. Oceanogr.*, **10**, 191–204, https://doi.org/10.1080/1755876X.2017.1307801.

Pao H. P., & Kao. T. W., 1977: Vortex structure in the wake of a sphere. *Amer. Inst. Physics*, **20**, 187–191.

Radko, T., & D. Lewis, 2019: The age of a wake. *Physics of Fluids*, **31**, 76601–. https://doi.org/10.1063/1.5100969.

Redford, J. A., Lund, T. S., and Coleman, G. N. 2015: A numerical study of weakly stratified turbulent wake. *Journal of Fluid Mechanics*, **776**, 568–609.

Spalart, P. R., W. H. Jou, M. Strelets, and S. R. Allmaras, 1997: Comments on the feasibility of LES for wings, and on a hybrid RANS/LES. *Advances in DNS/LES*, Greyden Press, 137–147.

Spedding, G. R., 1997: The evolution of initially turbulent bluff-body wakes at high internal Froude number. *J. Fluid Mech.,* **337**, 283–301, https://doi.org/10.1017/S0022112096004557.

Spedding, G. R., 2002: Vertical structure in stratified wake with high initial Froude number. *J. Fluid Mech.*, **454**, 71–112, https://doi.org/10.1017/S0022112001007182.

Spedding, G. R., 2014: Wake signature detection. *Ann. Rev. Fluid Mech.*, **46**, 273–302, https://doi.org/10.1146/annurev-fluid-011212-140747.

Tisovska, P., 2019: Description of the overset mesh approach in ESI version of OpenFOAM. *Proc. CFD with Open-Source Software*, H. Nilsson. Ed, http://dx.doi.org/10.17196/OS_CFD#YEAR_2019.

Voropayev S. I., Fernando H. J. S., Smirnov S. A., and Morrison R., 2007: On surface signatures generated by submerged momentum sources. *Physics of Fluids*, **19**, 076603, https://doi.org/10.1063/1.2749713.

Voropayev, S. I., C. Nath, H. J. S. Fernando, 2012: Thermal surface signature of ship propeller wakes in stratified waters. *Physics of Fluids*, **24**, 116603-, https://doi.org/10.1063/1.4767130.

Weller, H. G., G. Tabor, H. Jasak, and C. Fureby. 1998: A tensorial approach to computational continuum mechanics using object-oriented techniques. *Computers in Physics*, **12**, 620–631, https://doi.org/10.1063/1.168744.

Zappa, C. J., & A. T. Jessup, 2005 : High-resolution airborne infrared measurements of ocean skin temperature. *IEEE Geoscience and Remote Sensing Letters*, **2,** 146–150, doi: 10.1109/LGRS.2004.841629.

INITIAL DISTRIBUTION LIST

1. Defense Technical Information Center
   Ft. Belvoir, Virginia

2. Dudley Knox Library
   Naval Postgraduate School
   Monterey, California